Time-Resolved Small-Angle X-ray Scattering Study of the Kinetics of Disorder−Order Transition in a Triblock Copolymer in a Selective Solvent for the Middle Block

ARTICLE *in* MACROMOLECULES · SEPTEMBER 2003

Impact Factor: 5.8 · DOI: 10.1021/ma034357+

3 AUTHORS, INCLUDING:

Rama Bansil
Boston University
129 PUBLICATIONS **2,405** CITATIONS
SEE PROFILE

Kenneth R Ludwig
Berkeley Geochronology Center
158 PUBLICATIONS **9,636** CITATIONS
SEE PROFILE

Time-Resolved Small-Angle X-ray Scattering Study of the Kinetics of Disorder−Order Transition in a Triblock Copolymer in a Selective Solvent for the Middle Block

Huifen Nie, Rama Bansil,* and Karl Ludwig

Department of Physics, Boston University, Boston, Massachusetts 02215

Milos Steinhart and Čestmír Koňák

Institute of Macromoleculear Chemistry, Academy of Sciences of the Czech Republic, Heyrovsky Sq. 2, 162 06 Prague 6, Czech Republic

Joona Bang

Department of Chemical Engineering & Materials Science, University of Minnesota, Minneapolis, Minnesota 55455

Received March 20, 2003; Revised Manuscript Received July 24, 2003

ABSTRACT: The kinetics of the disorder−order transition (ODT) in a triblock of polystyrene (PS) and poly(ethylene-*co*-butylene) (PEB), in mineral oil, a selective solvent for the middle PEB block, was followed by time-resolved SAXS using both temperature ramp and rapid temperature quench techniques. Data analysis, using the Percus−Yevick interacting hard-sphere model plus Gaussians for the Bragg peaks in the ordered body-centered-cubic (bcc) state, shows that the core radius R_c, the hard-sphere volume fraction ϕ, and their interaction radius R_{hs} increased with decreasing temperature in the disordered state. At the ODT, ϕ reaches a maximum and R_c and ϕ change on ordering. The kinetics exhibits two stages corresponding to temperature equilibration and supercooling of the micellar fluid followed by nucleation and growth of the ordered state. The induction time for the onset of the second stage shows a minimum around the glass transition of the polystyrene cores.

I. Introduction

Recent studies on the phase behavior of styrene isoprene diblocks in selective solvents show that by tuning the solvent−polymer interactions it is possible to control their phase behavior and morphology.[1−3] The rich phase diagrams obtained suggest that examining the processes involved in the transitions between different ordered and disordered states in block copolymers in selective solvents is of obvious fundamental and practical interest. The understanding of the kinetics of micelle formation and of micellar ordering in block copolymer solutions is not as advanced as that of their equilibrium phase behavior, nor as advanced as the understanding of the kinetics of phase transitions in block copolymer melts.[4,5]

One common approach to study kinetics is the use of temperature ramp measurements to follow the structural changes in small-angle X-ray scattering (SAXS).[6−10] This is a convenient method to examine the phase diagram since discontinuities in peak intensity in a heating ramp can be used to locate the order−disorder transition (ODT) temperature T_{ODT}.[4] Several temperature ramp SAXS experiments on solution of triblock of polystyrene (PS) and poly(ethylene-*co*-butylene) (PEB), SEBS (PS−PEB−PS), in mineral oil show evolution of the body-centered-cubic (bcc) phase with decreasing temperature[8−10] and provide information about the temperature dependence of structural parameters of micelles.[8] However, it is important to note that in temperature ramp measurements the results depend on the rate of cooling or heating, and cooling ramps are further complicated due to effects of hysteresis and problems related to heat transport in the sample cell. Since the structural evolution is not isothermal, these results cannot easily be interpreted in terms of nucleation models. To best examine the isothermal kinetics of the ordering process, the temperature has to be rapidly changed to a temperature below T_{ODT} such that the new ordered state evolves by the mechanism of nucleation and growth.[11−13] The kinetics of nucleation and growth has been extensively studied in other systems, particularly in metallic alloys,[14] and is often described by the Avrami approach.[15−17] Temperature jump measurements using time-resolved SAXS have been reported in block copolymer melts[18−21]and diblock copolymer solutions.[22−25] Time-resolved SAXS study of the disorder−order transition in styrene−butadiene diblock copolymer solutions in selective solvents shows agreement with models of nucleation where defect-dominated growth mechanisms play a role.[22−24] However the temporal evolution of structural parameters such as micelle core radius and volume fraction was not obtained in these studies. SAXS data showing the time evolution of the intensity of the body-centered-cubic (bcc) peak in styrene−isoprene triblock[18] and of the disorder to cylindrical phase transition[26] has been reported, but no detailed analysis of the temporal evolution of the structural parameters was reported.

In this paper we focus on the kinetics of the transition from the disordered fluid to the ordered bcc state and present a detailed analysis of the structural changes during the ordering process in solutions of a triblock copolymer SEBS in mineral oil, a selective solvent for the middle PEB block. In this system the PS cores of

* Corresponding author: e-mail R.Bansil: rb@bu.edu.

10.1021/ma034357+ CCC: $25.00
Published on Web 09/16/2003

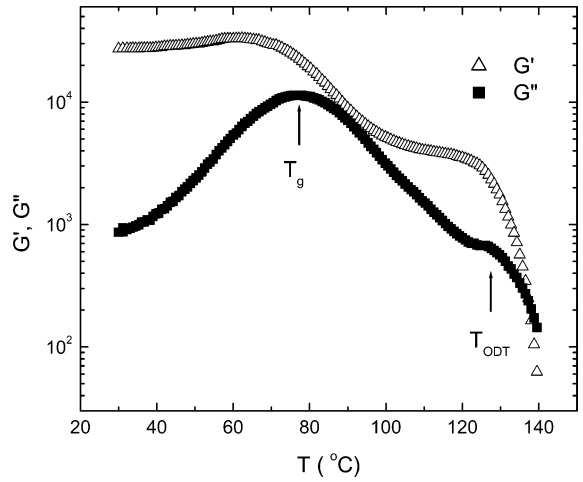

Figure 1. Dynamic shear moduli G' and G'' measured as a function of temperature with $\omega = 1$ rad/s, 1% strain amplitude at a heating rate of 1.5 °C/min. T_g and T_{ODT} are indicated on the graph.

the micelles are bridged by the soluble PEB block. We have previously examined heptane solutions of the same polymer samples used in this study by dynamic light scattering,[27] and a preliminary report on the kinetics of ordering in heptane solutions measured by time-resolved SAXS has been published.[28] By switching to mineral oil, we were able to slow down the kinetics as well as extend the temperature range over which measurements could be made, thus obtaining time evolution data for different temperatures over a considerably longer period. In this paper we analyze both temperature ramp and temperature jump measurements to follow the changes in the structural parameters and to evaluate the temperature dependence of the kinetics.

II. Experimental Section

II.1. Copolymer. A 20% w/v solution of the sample of SEBS triblock (Shell Chemicals, Kraton G1650 with a molecular weight M_n 100 000, polydispersity $M_w/M_n = 1.05$, styrene fraction 28 wt %, E:B ratio 1:1) was prepared by dissolving the polymer in mineral oil (a mixture of saturated naphthenic and paraffinic liquid hydrocarbons from petroleum, J.T. Baker). The mixture was heated at 180 °C for several hours until a clear solution was obtained. Mineral oil was used as the selective solvent for the middle block because it slows down the transition due to its high viscosity and also because several previous SAXS studies[10] have been reported on Kraton G1650 in a very similar oil, Fina Vestan A360. In earlier work we have examined the same polymer as well as a fractionated component of the same polymer in heptane, dioxane, and tetradecane.[28,29] We found that the SAXS and SANS data were qualitatively similar in both the fractionated and unfractionated sample, and have thus used the unfractionated block copolymer, because it was available in larger quantities. The copolymer was like a gel and was loaded into a custom X-ray scattering cell consisting of a copper plate of thickness 1 mm with a hole of diameter 0.6 cm covered with two thin flat Kapton windows. Sample cells were heated in an oven at 180 °C to remix the polymer as necessary.

II.2. Rheology. The dynamic shear moduli G' and G'' for the 20% sample as a function of temperature were measured at the University of Minnesota on an ARES rheometer (Rheometric Scientific) at a frequency of 1 rad/s, strain of 1%, and a temperature ramp rate of 1.5 °C/min. The results shown in Figure 1 are qualitatively similar to those reported in triblock copolymers[7,30] and reveal an ODT in the vicinity of 125−127 °C and a glass transition temperature T_g of 77 °C. As further evidence of glass transition effects, we note that samples quenched from the disordered micellar liquid state at 140 °C to temperatures below the T_g took a much longer time (∼2 days at 60 °C) to develop ordered structures than those quenched to temperatures above the T_g (∼1 h at 100 °C). To avoid possible complications due to the glass transition associated with polystyrene, we have restricted our temperature jump measurements to the temperature range of 80−140 °C.

II.3. Small-Angle X-ray Scattering. The kinetic SAXS measurements were carried out at X27C beamline of the National Synchrotron Light Source (NSLS) at Brookhaven National Laboratory. The X-ray wavelength was 0.1366 nm (9.01 keV) with energy resolution $dE/E = 1.1\%$. By using a one-dimensional linear position-sensitive EMBL wire detector with 512 channels, the entire scattering intensity profile $I(q)$ could be recorded in a single measurement. Here $q = (4\pi/\lambda) \sin\theta$ denotes the magnitude of the scattering vector with 2θ being the scattering angle. The sample-to-detector distance was 1.95 m, which covers the range $0.01 < q < 0.3$ Å^{-1}. The exact q calibration was calibrated using Ag behenate ($d = 5.8$ nm) as a standard. Aluminum foils were placed in front of the detector to attenuate the beam to prevent possible damage to the detector due to high intensity. All data were normalized to constant incident intensity using the ionization chamber current, which is proportional to the primary beam intensity, corrected for transmission of the sample by monitoring the transmitted intensity on a photodiode mounted at the beam-stop. In the WAXS region, which was also examined by a second EMBL wire detector, there was no significant structural information. However, the total WAXS scattering was useful for determining the attenuation of the beam by the aluminum foils placed in the beam path.

Two different temperature jump apparatus were used over the course of this study: (i) an air-cooled dual-cell temperature jump apparatus and (ii) a single cell with a Peltier heater/cooler to change the sample temperature rapidly. The former has the advantage of a slightly faster temperature equilibration time, while the latter provides a better stability of the final temperature as well as the ability to both heat and cool. Typically, the final temperature is reached within 60 s for the dual cell apparatus and 200 s for the Peltier device. The temperature was monitored by using a thermocouple placed in the sample as close to the beam as possible.

To determine the equilibrium structure, the sample was equilibrated at the desired measuring temperature for at least 2 h prior to the measurement. Static scattering measurements were made by averaging the scattered intensity profiles $I(q)$ for 10 min. To follow the kinetics by time-resolved SAXS measurements, $I(q;t)$ was measured with a short exposure time throughout the ordering process. Two different approaches were used to examine the kinetics: (i) *temperature ramp*: the temperature was varied from the initial to the final value at a constant rate; (ii) *temperature jump*: the temperature was rapidly changed from an initial to a final value and held constant thereafter. Temperature jumps with different quench depth were measured for 1 or 2 h runs with exposure time of 10 s per frame for the first 60 frames to capture the early stages of the kinetics and the subsequent frames recorded with an exposure time of 60 s per frame.

II.4. Model for Analysis of SAXS Data. To model the scattering from a network of bridged and/or looped micelles such as those formed in a triblock copolymer in a selective solvent for the middle block, one has to deal with the interactions between micelles mediated by both hard-sphere repulsion and those due to the chains. Some attempts at including these interactions have been considered in analyzing structure factors of isolated diblock copolymer micelles. For example, an attractive square well[31] has been used to describe hard-core repulsion. Pedersen[32] has provided a review of many possible potentials applicable to colloidal systems. Since it is not clear which potential to use for our system, we have taken the simplest approach of using the Percus−Yevick interacting hard-sphere potential.[33] This approach has been used to calculate the structure factors for spherical micelles in the fluid state as an effective system of interacting hard spheres.[34−38]

The scattering intensity from a monodisperse system of particles can be written as a product of the single particle form factor $P(q)$ and a structure factor $S(q)$, describing the interparticle interference:

$$I(q) = I_0 P(q)\, S(q) \tag{1}$$

where I_0 depends on the contrast factor and the number density of scatterers.

We use the spherical form factor approximation for $P(q)$, assuming that the cores are spherical with radius R_c, and the Percus−Yevick structure factor $S(q)$ to describe their excluded-volume interaction, which is a function of the hard-sphere volume fraction ϕ and the hard-sphere interaction radius R_{hs}.[35] Thus, the scattering intensity from the micelles in the disordered liquid phase is a function of ϕ, R_c, and R_{hs}. On the other hand, in the ordered phase the micellar cores are on a lattice and give rise to Bragg peaks. The scattering from the Bragg peaks is represented by a sum of Gaussians $\sum_i A_{G,i}(t)e^{-(1/2)[(q-q_i)/\sigma_i]^2}$ with $A_{G,i}$, q_i, and σ_i denoting the amplitude, position, and width of the ith Gaussian peak, respectively, as have been used in the literature.[22,23] The position of only the first Bragg peak q_1 was treated as a fitting parameter; the positions of the remaining Bragg peaks were determined in terms of q_1 using the appropriate crystalline symmetry.

The observed scattering $I(q,t)$ during the phase transformation at time t is made up of the coexisting disordered and ordered phases and can be written as

$$I(q,t) = I_{disorder}(q,t) + I_{order}(q,t) \tag{2}$$

where $I_{disorder}$ given by eq 1 is the scattering due to the fraction in the disordered phase at time t and I_{order} is the scattering from the fraction in the ordered phase at time t, represented by a sum of Gaussians. Since the Gaussian peaks are quite narrow, the spherical form factor does not vary significantly over a given Bragg peak. However the form factor's effect was taken into account in comparing the amplitudes of the different Gaussian peaks. The data were fit to the model described above using four parameters, I_0, R_c, R_{hs}, and ϕ, to describe the scattering from the disordered phase and seven parameters, q_1, $A_{G,i}$, and σ_i (i = 1, 2, 3), to model the scattering from the ordered microdomains. We used either the full model (eq 2) with 11 parameters when higher order Bragg peaks were present or just the Percus−Yevick model with four parameters when there is only liquidlike short-range order in the system. Polydispersity effects can be taken into account by adding for example a Gaussian distribution of core sizes. We have not included this in order to keep the number of parameters to a minimum. Core−shell models provide a more realistic description of block copolymer micelles and have been used to model the scattering from diblock micelles. Since in the bridged triblock system considered here the core and corona may not be very well-defined, we have restricted ourselves to the sphere form factor. For the same reason we have not used actual scattering length densities of the two blocks to obtain absolute intensities.

The fitting was done in two steps. First, a program using the genetic algorithm[39] was used to get a reasonably good fit. The program runs faster than conventional algorithms but cannot reach a very good fit, so further fitting procedures had to be carried out using the parameters from the first step as initial guesses. The second fitting was done using the nonlinear least-squares fitting program based on the Levenberg−Marquardt algorithm[40] in the software package Origin. This algorithm also provides estimate of the error bars of the fitting parameters.

As an alternative to using the Percus−Yevick model, a simpler purely phenomenological approach is to treat the scattering from the liquid as a Lorentzian in the vicinity of the first peak and that from the ordered phase as a sum of Gaussians. This approach was used by Harkless et al.[22] to analyze the kinetics in a diblock copolymer solution. We compared the results of the Percus−Yevick model with the Lorentzian model and found that the fit was significantly better using the Percus−Yevick model. Furthermore, Harkless et al.[22] did not include the spherical form factor, so they could not obtain the time evolution of micelle structural parameters. However, we have also used a Lorentzian line-shape analysis in addition to the Percus−Yevick analysis to characterize the change in the primary peak's position intensity and width.

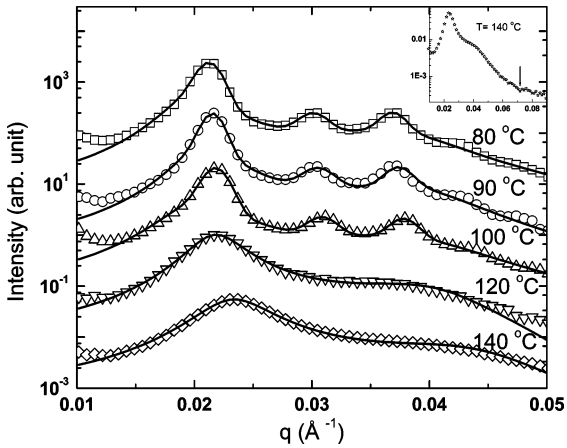

Figure 2. Scattering intensity $I(q)$ vs q from 20% SEBS in mineral oil at different temperatures as indicated. The data are offset by factors of 10 for clarity. The solid lines are the results of the fit to eq 2. The inset covering the q range from 0.01 to 0.09 Å^{-1} shows a minimum around 0.071 Å^{-1} as indicated by the arrow for the data at 140 °C.

III. Results and Discussion

III.1. Static Structure Factor of Semidilute Triblock Copolymer Solutions. Although the equilibrium structure of SEBS has been extensively investigated,[6,8−10,41] we present the equilibrium data and its analysis because it is important to establish the initial and final values of the structural parameters in the liquid and ordered states prior to following their temporal evolution. Figure 2 shows the scattering intensity $I(q)$ from a 20 wt % triblock sample in mineral oil at different temperatures. At 140 °C, $I(q)$ shows one well-formed maximum in the structure factor at q_{max} = 0.023 Å^{-1} and a shoulder near 0.04 Å^{-1}, which become more pronounced as the temperature decreases to 120 °C. Similar scattering behavior has been observed in many block copolymer micellar systems with PS cores[10,35] and attributed to the short-range ordering of micellar cores. As mentioned above, a reasonable description of these features can be given in terms of the Percus−Yevick hard-sphere model.[35] The fit of the data to this model in the q range of 0.01−0.05 Å^{-1} are also shown in Figure 2. The fit works well except that small deviations from the model are observed at the two ends of this range. The parameters R_c, R_{hs}, and ϕ are determined to an accuracy of about 2.5 Å, 1.5 Å, and 0.015, respectively, when there is only micellar liquid, and 0.5 Å, 0.2 Å, and 0.0015, when Bragg peaks are present.

An independent estimate of R_c can be obtained from the position of the first minimum in the form factor via the relationship $q_{min} = 4.49/R_c$. The inset of Figure 2 shows that q_{min} is around 0.071 Å^{-1} at 140 °C, which gives R_c = 63 Å, in reasonable agreement with the fitting results. The parameters of the fits (Table 1) are comparable with those of Kleppinger et al.[10] on the same system in a similar solvent (FINA Vestan A360) at similar concentration.

As the temperature is further decreased to 100 °C, higher order Bragg peaks show up at $q/q_1 = 1, \sqrt{2}, \sqrt{3},$

Table 1. Structural Parameters for 20% SEBS in Mineral Oil Obtained by Fitting the Static SAXS Measurements to the Model Described in the Text

T (°C)	R_c (Å)	R_{hs} (Å)	ϕ	q_{max} (Å^{-1})	q_1 (Å^{-1})	a_{bcc} (Å)	d_{nn} (Å)	$f_{disorder}$
80	69	169	0.42	0.0210	0.0213	417	361	0.029
90	70	161	0.44	0.0217	0.0216	411	356	0.036
100	67	160	0.39	0.0217	0.0218	407	352	0.029
120	77	155	0.45	0.0217			361	0.055
140	69	141	0.41	0.0237			331	0.048

$\sqrt{4}$, and $\sqrt{5}$. Even a sixth peak can be identified in some of the data (e.g., the 90 °C data). We observe that the second peak is lower in intensity compared to the third peak. This further supports the bcc structure, since the multiplicity of the third Bragg peak is higher than that of the second one in the powder pattern of a bcc crystal.[42]

In the Percus−Yevick model the position of the maximum in the primary peak, q_{max} is a function of both ϕ and R_{hs}, with the peak intensity being more strongly dependent on ϕ and the peak position on R_{hs}. For hard-sphere liquids $d_{nn} \sim 2.5\pi/q_{max}$, where d_{nn} is the nearest-neighbor distance, whereas for the bcc lattice, $d_{nn} = \sqrt{6}\pi/q_1$. This value is given in Table 1 and shows that d_{nn} in both the liquid and ordered phase is close to $2R_{hs}$. Table 1 also gives the value of the bcc lattice constant $a_{bcc} = 2\sqrt{2}\pi/q_1$.

We have estimated the volume fraction of the cores in the disordered phase using the relation $f_{disorder} = \phi R_c^3/R_{hs}^3$. We find that at 120 °C the volume fraction of cores in the liquid state, $f_{disorder} = 0.055$, is very close to the total available volume faction of PS of 0.0549, calculated for the 20% sample with 28% PS (using the density $\rho_{PS} = 1.02$ g/cm^3), which suggests that most of the PS chains aggregated into micelles at this temperature. At temperatures below the ODT both ordered and disordered phases coexist. This calculation is based on rather simplistic assumptions, such as cores made of pure PS, no polydispersity, no density changes in PS, and a clear demarcation between disordered and ordered phases; thus, it should be viewed as a rough estimate. However, it does indicate a substantial coexistence of ordered and disordered phases in this sample.

III.2. Temperature Ramp Measurements. As mentioned earlier, the ODT can be determined from a heating ramp. Although detailed analysis of the temperature dependence of the micellar structural parameters from heating ramps has been reported,[8,34] to the best of our knowledge there is no detailed analysis on cooling ramps. One key issue with temperature ramp measurements that has not been addressed much in the literature is the dependence on the ramp rate and the direction (heating vs cooling). In the following, we discuss the results from a series of heating and cooling ramps with varying rates.

III.2a. Determination of the ODT from a Heating Ramp. The ODT of the sample was located using a temperature ramp from 60 to 140 °C at 4 °C/min. For this measurement 40 frames with 30 s exposure each and no delay between the frames were recorded. As is well-known,[4] a discontinuity in the peak scattering intensity can be seen in the plot of $1/I_{max}$ vs $1/T$ in the vicinity of the ODT. As shown in Figure 3, the discontinuity for this sample is between 117 and 121 °C, giving an ODT near 119 °C. This value compares reasonably well with SAXS measurements reported in the literature on similar samples.[8,43] The figure also shows that the full width at half-maximum of the peak, obtained by a Lorentzian fit over a narrow interval around the peak, increases rapidly at the ODT.

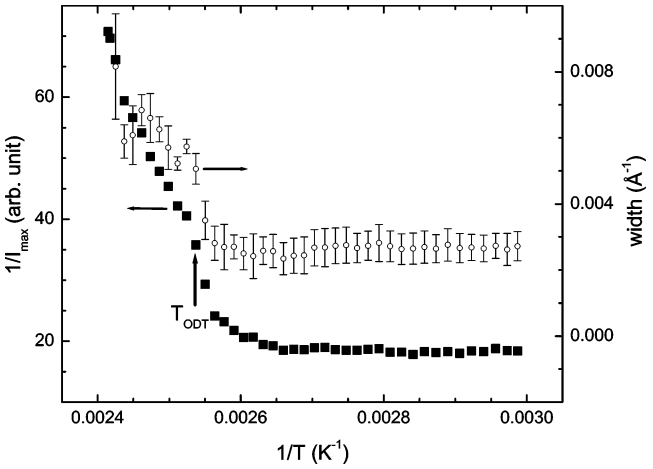

Figure 3. Full width at half-maximum (open symbol) and inverse peak intensity $1/I_{max}$ (filled symbol) as a function of inverse temperature $1/T$ in a heating ramp from 60 to 140 °C at 4 °C/min. T_{ODT} is indicated on the graph.

III.2b. Effects of Varying Ramp Rate. To examine the effects of varying ramp rate on the structural changes of the system, we conducted two cycles of ramps: one from 90 to 140 °C (H1) and then back to 90 °C (C1) at 0.3 °C/min; the other from 40 to 140 °C (H2) and then down to 70 °C (C2) at 1 °C/min. We also carried out a heating ramp from 60 to 140 °C (H3) at 4 °C/min and two cooling ramps, one from 140 to 60 °C (C0) at 0.33 °C/min and the other from 140 to 20 °C (C3) at 2 °C/min. Parts a and b of Figure 4 show the temperature dependence of the maximum intensity from these heating and cooling ramps, respectively. The two cycles, H1−C1 and H2−C2, clearly show the effects of hysteresis; i.e., the maximum intensity in the cooling process does not recover to that in the corresponding heating process, as can be seen from the inset of Figure 4b. However, over the temperature range where the system is in the micellar liquid state, the data from the heating and cooling are almost coincident, indicating that hysteresis effects are more pronounced in the crystalline state. Another significant feature is the overlap of the data for all the cooling and heating ramps, irrespective of ramp rate, within certain temperature windows. The range of overlap for the heating ramps is 120−140 °C, reflecting the fast kinetics of the order−disorder transition and the ability of the system to respond quickly to temperature change in the micellar liquid state. In comparison, the cooling ramps appear to be insensitive to the rate of cooling in the range of 140−95 °C, a wider temperature interval than that seen in the heating ramps, possibly related to the supercooling of the disordered structure in these cooling ramps. We also noted that the kinetics of ordering transition is slower as compared to that in the disordering process; i.e., the ordered phase requires longer time to develop.

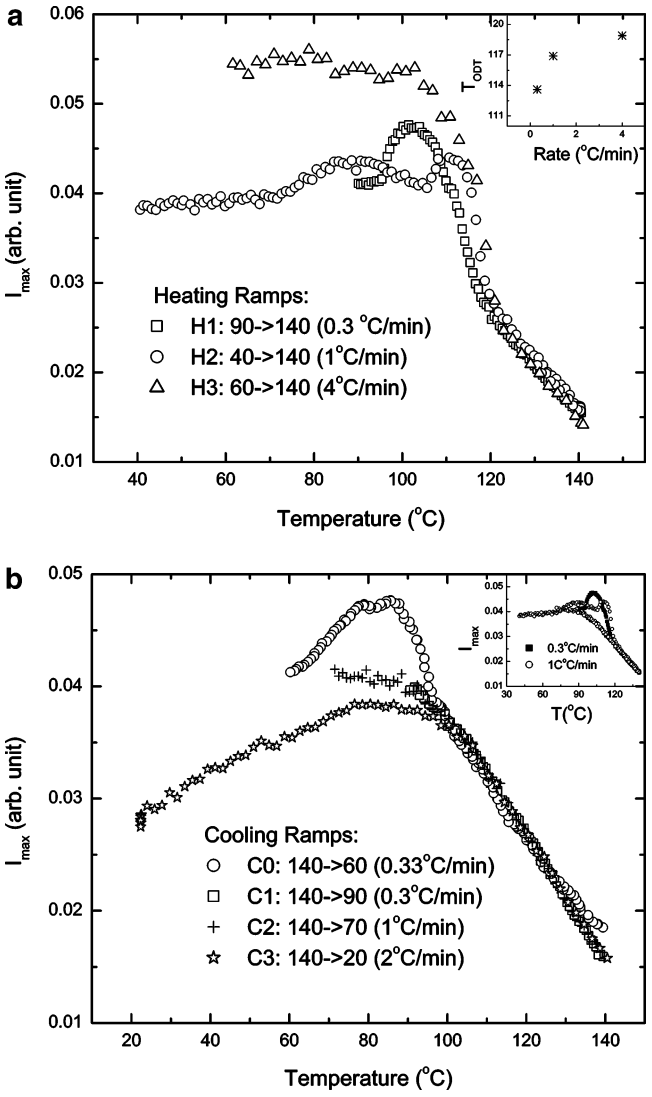

Figure 4. (a) Maximum intensity (I_{max}) vs temperature from a series of heating ramps at various ramp rates as indicated. The heating ramps are labeled as H1, H2, and H3, with ramp rate of 0.3, 1, and 4 °C/min, respectively. The inset shows the dependence of T_{ODT} on the ramp rate. (b) Maximum intensity (I_{max}) vs temperature from a series of cooling ramps at various ramp rates as indicated. The cooling ramps are labeled as C0, C1, C2, and C3, with ramp rate of 0.33, 0.3, 1, and 2 °C/min, respectively. Note that C0 was measured earlier than the rest of the experiments, on the same beamline with slightly different experimental setup, so the intensity data are linearly scaled. The inset shows hysteresis effects in I_{max} from the two cycles H1−C1 and H2−C2.

The data for the heating ramp H2 display two maxima, with the first one corresponding to the glass transition of polystyrene and the second one corresponding to the best ordered bcc structure of the micelles. In contrast, the data for H1 exhibit just one maximum since the starting temperature 90 °C is above T_g. Note that the intensity from ramp H3 is higher than that from the other two heating ramps due to the fact that the sample was annealed at 60 °C for about 2 days prior to the experiment and that it also does not show any well-resolved maximum as seen in the other two heating ramps. The height of the peak above T_g decreases as the ramp rate increases as expected, since the slower the rate, the longer the time available for the ordered crystalline structure to grow. As shown in the inset of Figure 4a, the T_{ODT} as evaluated from the heating ramps does not vary linearly with the ramp rate. In principle, the real T_{ODT} could be obtained by extrapolating the data to a ramp rate of zero, if there were more measurements. Our data suggest that this extrapolated T_{ODT} is around 112 °C. Finite heating rate gives higher value of T_{ODT}; the higher the rate, the greater the discrepancy.

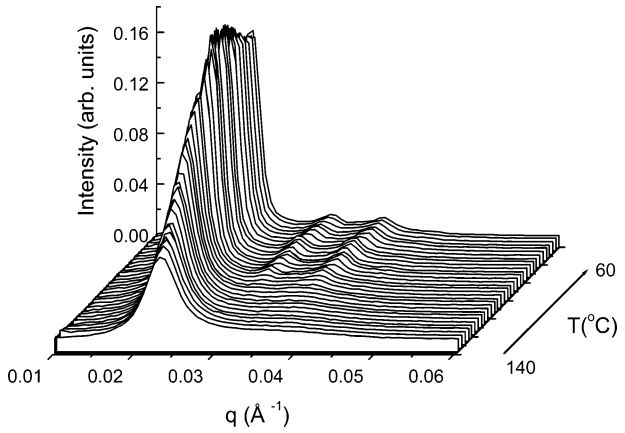

Figure 5. Temperature dependence of the scattering intensity $I(q)$ vs q during a cooling ramp from 140 to 60 °C.

For the cooling ramps, ordered structure developed only in C0. The difference between C0 and C1, which has a similar rate, could be related to the smaller temperature range of C1 (only down to 90 °C) and/or the differences between the two samples and their thermal history. The ramps C2 and C3 are probably too fast to allow sufficient time for the ordered structure to develop.

In the following section, we present a detailed analysis of the data from the cooling ramp C0 since ordered structures appeared only in this cooling ramp. We focused on analyzing cooling ramps because the temperature dependence of the structural parameters in cooling is relevant to interpreting temperature jump experiments discussed later.

III.2c. Phenomenological Analysis of Cooling Ramp Data. SAXS data for the 20% sample in mineral oil taken from the cooling ramp C0 are shown in Figure 5; this shows clear appearance of secondary Bragg peaks at $\sqrt{2}q_1$ and $\sqrt{3}q_1$ below 103 °C. The Bragg peaks grow in intensity until the temperature cools to 90 °C. There are also obvious changes in peak width and a slight change in peak position. To put the qualitative observations of changes in peak intensity, position, and width on a more quantitative footing, we estimate the peak intensity, position, and full width at half-maximum by a simple Lorentzian line shape analysis of the data in a narrow interval around the maximum. It should be pointed out that this analysis is a phenomenological way to obtain peak parameters; it does not imply that a Lorentzian structure factor describes the correct physics.

Figure 6 shows the temperature dependence of peak intensity, width, and peak position. Also shown on the graphs are the results of a similar analysis for the static ("equilibrium") data. As the sample is cooled, the width decreases until ~90 °C, as expected for a system which goes toward an ordered state. The peak intensities of the samples annealed at 140 and 120 °C for longer times are almost equal to those seen in the ramp experiment at these temperatures, implying that structural rear-

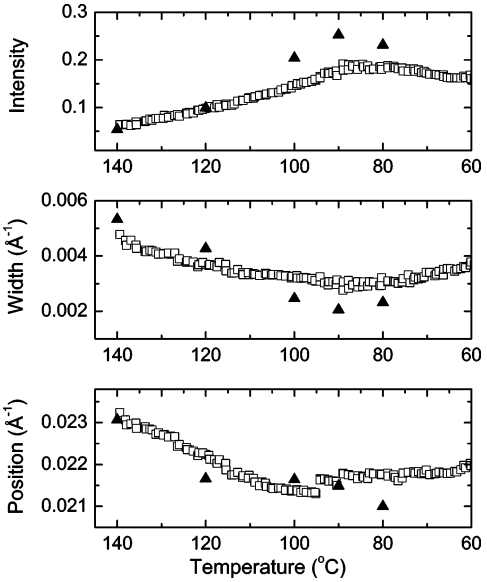

Figure 6. Temperature dependence of the peak intensity, position, and full width at half-maximum from a Lorentzian fit over a narrow interval around the peak to get a phenomenological understanding of the evolution of the primary peak for the ramp from 140 to 60 °C. The filled triangles are the fitted results for static measurements. Note that the temperature axis is reversed to point in the direction of cooling.

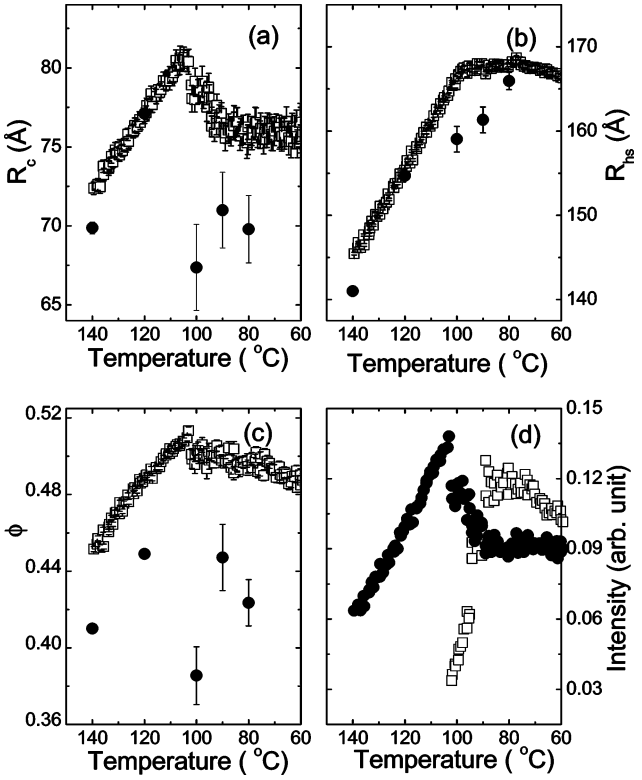

Figure 7. Temperature dependence of the micellar parameters for the cooling ramp from 140 to 60 °C: (a) the core radius, R_c; (b) the hard-sphere interaction radius, R_{hs}; (c) the volume fraction of hard spheres, ϕ; and (d) first Bragg peak amplitude $A_{G,1}$ (open symbol) and maximum intensity for $I_{disorder}$ (filled symbol). The filled circles in (a), (b), and (c) are the fitted results for static measurements. Note that, as in Figure 5, the temperature axis is reversed.

rangement occurs quite rapidly while the sample is in the liquid phase. In contrast, the intensities measured during a cooling ramp at temperatures where the sample is in the ordered state are lower than those measured after a longer annealing time. This is to be expected because it takes time for the ordered structure to grow. As seen in Figure 6, the peak intensity and width appear to go through a shallow extremum around 90 °C, a maximum for the intensity and a minimum for the width. This behavior is most likely related to the formation of glassy PS cores in this temperature regime. The actual position of this extremum would be dependent on the rate of cooling.

III.2d. Analysis of Temperature Ramp Data Using Percus−Yevick Model. The structural parameters describing the micellar system were obtained by the least-squares fitting of the scattering intensity data to eq 2 in the q range of 0.01−0.05 Å^{-1}. At temperatures below 103 °C where a second Bragg peak could be identified, we included Gaussians to describe the Bragg scattering from the ordered lattice. From the fits we obtained information on the micellar core radius, hard-sphere interaction radius, and hard-sphere volume fraction as a function of temperature. The results obtained for the cooling ramp from 140 to 60 °C are shown in Figure 7.

The volume fraction occupied by the effective hard spheres increases in the liquid phase, reaching a maximum value of about 0.52, and shows a small but sudden drop when the system goes through the ODT. A similar value of 0.53 was observed in the ordering of a poly(ethylene oxide)-*block*-poly(propylene oxide)-*block*-poly(ethylene oxide) triblock copolymer.[44,45] The micellar core radius R_c and the hard-sphere radius R_{hs} both increase as the temperature decreases below 140 °C in the liquid phase. This probably reflects increase in the aggregation number of micelles but can also be partly due to the change in micelle size due to conformational changes of the polymer chains. From 100 °C downward, R_{hs} is almost constant (or decreases very slightly) while the micellar core radius R_c exhibits a sharp but small decrease when the sample enters the cubic phase and is almost unchanged below 90 °C. The decrease in core radius on entering the cubic phase may be due to the formation of a better defined core in the ordered phase or due to the expulsion of solvent from the cores. Two other features are worth pointing out. First, since the rate of cooling is faster than the rate at which the system transforms, the liquid will supercool, so that the apparent transition temperature seen in a cooling ramp is lower than the actual ODT. Second, all the parameters for the samples "equilibrated" at fixed temperatures are lower than those seen in the ramp, reflecting the time needed for the ordered phase to grow.

Figure 7d shows that, as the temperature decreases, the calculated peak intensity of the Percus−Yevick part (the first term in eq 2) decreases quite rapidly while the amplitude of the first Bragg peak increases as the temperature goes below the apparent ODT. As has been previously observed,[7] there is no discontinuity in the primary peak intensity in a cooling ramp; however, the peak amplitude of the Percus−Yevick component exhibits a gradual drop as the temperature goes through the ODT.

III.3. Temperature Jump Measurements. Temperature jump kinetics was measured by rapidly varying the temperature of the sample from 140 °C to several different final temperature values. The results were qualitatively similar for the different quenches. In addition to these cooling jumps, heating jumps were also examined. However, the disordering transition was

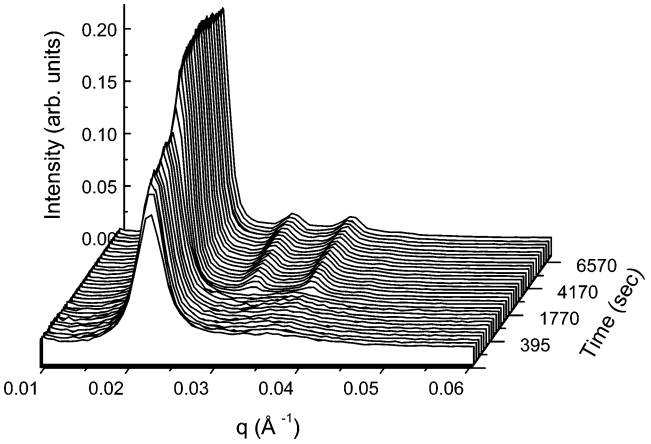

Figure 8. Time evolution of the scattering intensity $I(q)$ vs q following a jump from 140 to 96 °C.

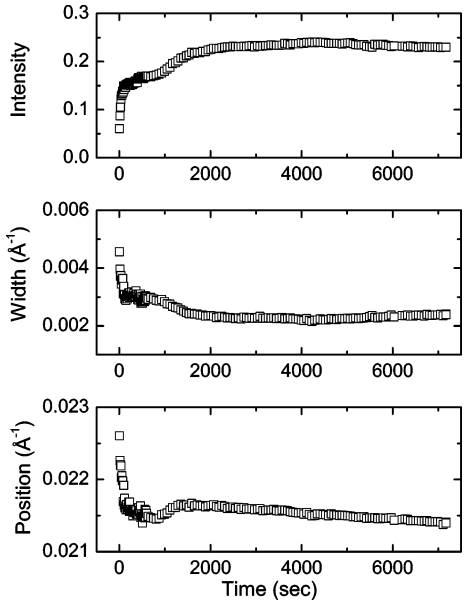

Figure 9. Time evolution of the peak intensity, position, and full width at half-maximum from a Lorentzian fit over a narrow interval around the peak for the quench from 140 to 96 °C.

much faster than the ordering process; the former took only 200−250 s to go to completion whereas the latter took hours. For this reason, all further analysis and discussions is on cooling jumps. Figure 8 shows the typical time evolution of the scattered intensity following a quench from 140 to 96 °C for 20% sample in mineral oil. The temperature reached 96 °C within 90 s after the jump and thereafter remained at 96 ± 0.5 °C. After the temperature has equilibrated the time evolution clearly shows two stages: an initial stage (lasting for ∼1000 s) where the peak intensity grows slowly and higher order peaks are not present and a later stage where the peak intensity increases rapidly and well-defined Bragg peaks can be seen.

III.3a. Phenomenological Analysis of Temperature Jump Data. As in the case of static and ramp data, a simple Lorentzian line shape analysis of data for the primary peak in the q range 0.01−0.022 Å^{-1} was also performed for the jump data, and the results are shown in Figure 9. The very fast change of the peak parameters in the first 100 s is due to the change in temperature. After the temperature stabilized, the peak intensity slowly increases, reaching a plateau at about

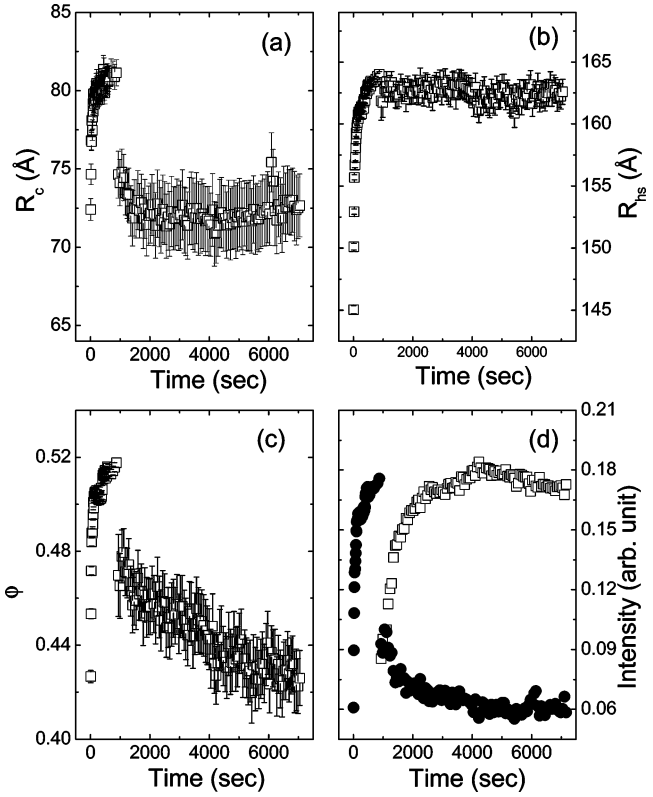

Figure 10. Time evolution of the fitted micellar structural parameters for the quench from 140 to 96 °C: (a) the core radius, R_c; (b) the hard-sphere interaction radius, R_{hs}; (c) volume fraction of hard spheres, ϕ; and (d) first Bragg peak amplitude $A_{G,1}$ (open symbol) and maximum intensity for $I_{disorder}$ (filled symbol).

1000 s, while the width narrows. During the first stage the peak position shifts to lower values. The greater noise for the earliest measurements is related to the fact that the first 60 frames were recorded with a 10 s averaging time whereas the later frames were recorded with a 60 s exposure time. Since no higher Bragg peaks were seen in the first 1000 s, we suggest that during this time the micellar fluid supercools. The trend of the parameters with time is the same as the trend in a cooling ramp (see Figure 6), signaling the growth of the micelles either from the merger of small micelles into bigger ones or from the aggregation of free chains into new micelles. In the second stage higher order Bragg peaks develop at relative positions of 1:√2:√3, clearly revealing a cubic structure.

III.3b. Time Evolution of Micellar Structure Following a Jump. To get a quantitative analysis of the structural parameters for the ordering process, we fit the scattering data in the range 0.01−0.05 Å^{-1} to the model of coexisting liquid and ordered phases (eq 2). For later frames where Bragg peaks are developed, we used the full model (eq 2) with 11 parameters. We started the fitting from the last frame and used the fitting results from one frame as the initial guess for the next one. When the fitted width for the Gausian peaks underwent an abrupt increase, we switched to the Percus−Yevick model (eq 1) with four parameters. The time dependence of the micellar structural parameters R_c, R_{hs}, and ϕ is plotted in Figure 10. All three parameters exhibit rapid growth in the first 100 s while the temperature is equilibrating, followed by a smaller increase up to the point when higher order Bragg peaks develop, consistent with a supercooling of the disordered

phase. The volume fraction grows rapidly at early times up a maximum value of about 0.53, which has been shown to be the maximum volume fraction for hard-sphere crystal formation in triblock copolymer solutions[34,45] and colloidal crystallization.[46] When the volume fraction for hard-sphere crystallization is reached, the Percus−Yevick model does not work; we have to include the Gaussians due to the Bragg peaks. This change in the fitting model could cause the abrupt change in both the core radius and volume fraction seen in Figure 10. As the sample goes past the transition the slight decrease in the core radius is within the error bars of the fit, while that in the volume fraction is somewhat larger. Whether these changes are due to calculational artifacts or related to structural changes in the micelle is not possible to say with any degree of confidence given the simplistic model used here. On the other hand, the hard-sphere interaction radius remains fairly unchanged, indicating that it is more dependent on the conformation of the PEB chains which both tether to the PS core and act as bridges between the core. Shown in Figure 10d is the time evolution of the first Bragg peak intensity and the intensity at the maximum of the Percus−Yevick interaction peak. The higher Bragg peaks (not shown in the figure) also exhibited a similar growth in their peak intensities. These parameters also reflect the two-stage character of the transformation kinetics, with the increasing Percus−Yevick peak intensity corresponding to the supercooling process, followed by the ordering process during which the Bragg peak corresponding to ordered state grows while the Percus−Yevick component corresponding to the disordered state diminishes.

Two-stage transformation kinetics was observed in previous time-resolved SAXS studies on diblock copolymer solutions undergoing a transition from a homogeneous polymer solution to an ordered micellar state.[22] In those experiments the first stage reflects changes due to the formation of micelles (i.e., the microphase separation transition) as well as supercooling, whereas in our case, micelles are already present in the system initially, so the first stage reflects primarily the supercooling of the micellar fluid. The growth of the ordered phase in our case is very similar to the results seen in the diblock kinetics.

In contrast to the two-stage behavior in the ordering process, the disordering transition, which we examined by a heating jump from 90 to 140 °C, showed only one stage corresponding to the melting of the ordered domains. The process was too fast to perform a detailed analysis of the data.

III.3c. Quench Depth Dependence of the Kinetics of Nucleation and Growth. To investigate the effect of quench depth on the ordering kinetics, we carried out a series of temperature jump experiments from T_i = 140 °C to differing final temperatures T_f. Temporal evolutions of the primary peak intensity during these quench experiments are shown in Figure 11. At T_f = 112 °C, no ordering was observed during the 2 h run of the experiments although the temperature is lower than the ODT. For all the other quenches, the two-stage development of the primary peak intensity is clearly seen. The value of the maximum peak intensity is dependent on the final temperature of the quench; the lower the final temperature, the higher the maximum peak intensity. The onset of the second stage in the growth process is dependent on both the quench depth and the final temperature, reflecting the competition between the two factors that affect the ordering process, i.e., the thermodynamic driving force that is proportional to the quench depth and the final temperature which determines the mobility of the copolymer chains.

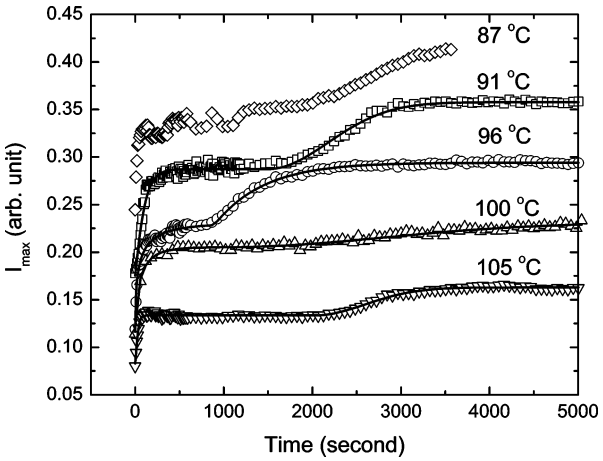

Figure 11. Temporal evolution of the primary peak intensity following quenches from 140 °C to different final temperatures, as indicated on the graph. The solid lines are fits to eq 7. The data are offset by different constant for clarity. The data at 87 °C are not fitted due to the incomplete growth of the ordered phase. Note that the data for the 100 °C quench also show the two-stage growth, but this feature is not apparent here due to the compressed vertical axis.

From these data we obtain information about the kinetics of the ordering process. The two-stage growth process is modeled as a sum of two growth processes

$$I_{max}(t) = I_{max1}(t) + I_{max2}(t) \quad (3)$$

where I_{max1} denotes the change in intensity during the supercooling and temperature equilibration and I_{max2} represents the nucleation and growth of the ordered phase after an induction time t_0. For the first stage we use a single-exponential relaxation term since equilibration of both temperature and concentration fluctuations[47] are expected to be approximately exponential relaxation processes of the general form

$$I_{max1}(t) = I_1(1 - e^{-k_1 t^n}) \quad (4)$$

For the second stage, which represents the nucleation and growth of the ordered state, we use the Johnson, Mehl, and Avrami transformation theory,[14] which predicts that, for a nucleation and growth process, the volume fraction of the transformed phase η should be

$$\eta = 1 - e^{-k(t-t_0)^n} \quad (5)$$

where the growth rate k and the exponent n characterize the rate of the transformation and the dimensionality and type of the growth process.[14] Usually the first-order Bragg peak $A_{G,1}(t)$ intensity is analyzed to determine the fraction of material in the ordered state. Since the fitting procedure (eq 2) does not work well in the earliest stages when the Bragg peaks are weakly developed, the fitted value of $A_{G,1}(t)$ does not reflect the true early growth of the Bragg peak. To overcome this problem, we determined the nucleation and growth kinetics by fitting the primary peak intensity as a sum

Table 2. Kinetic Parameters Describing the Two-Stage Growth in the Disorder-to-Order Transition for 20% SEBS in Mineral Oil, Using the Model Described in the Text

T_f (°C)	I_0	I_1	k_1	I_2	k_2 (10^{-5})	n	t_0 (s)	$t_{induction}$ (s)
91	0.0772	0.1009	0.0088	0.0697	0.1352	2	1600	2190
96	0.0646	0.0926	0.0226	0.0768	0.0850	2	300	930
100	0.0994	0.0765	0.0113	0.0249	0.0286	2	1600	2850
105	0.0856	0.0474	0.0341	0.0307	0.1368	2	2000	4530

of the contribution from the ordered and disordered phases

$$I_{max2}(t) = (1 - \eta)I_{max}^{disorder} + \eta I_{max}^{order} = I_{max}^{disorder} + \eta(I_{max}^{order} - I_{max}^{disorder}) \quad (6)$$

Thus, the two-stage development of the peak intensity can be written as

$$I(t) = I_0 + I_1(1 - e^{-k_1 t}) + I_2(1 - e^{-k_2(t-t_0)^n}) \quad (7)$$

where $I_2 = I_{max}^{order} - I_{max}^{disorder}$ denotes the difference in the contribution to the peak intensity from the ordered and disordered liquid at the completion of the ordering process. The results of fitting eq 7 to the data shown in Figure 11 are shown in the figure and summarized in Table 2. The first process is faster and saturates well before the time t_0. The growth rate during the supercooling stage, k_1, decreases as the final temperature decreases, reflecting the slowing down of the mobility with decreasing temperature. The induction time t_0 of the ordering process is minimum at 96 °C. We suggest that this reflects the competition between the increased driving force for ordering with increasing quench depth, and the decreasing mobility as the final temperature decreases. Since the PS cores of the micelles are approaching a glass transition at 77 °C, the mobility decrease should be quite pronounced. The value of t_0 obtained in the fitting procedure agrees reasonably with the induction time, $t_{induction}$, estimated by the appearance of the Bragg peaks. The growth exponent $n = 2$ indicates that the system exhibits site-saturated nucleation (i.e., all nucleation occurring at the beginning) followed by growth. The behavior of the growth rate k_2 is complicated, since it depends on several parameters, and it is difficult to say anything about its temperature dependence with the limited data. Somewhat similar behavior had been seen in metallic alloy[48] and copolymer solutions.[18]

IV. Conclusion

The kinetics of the ordering transformation in solutions of the PS−PEB−PS triblock copolymer in mineral oil was sufficiently slow to be monitored by time-resolved SAXS measurements following a rapid temperature jump or during a temperature ramp. The micellar structural parameters, namely the core radius, the volume fraction of hard spheres, and their interaction radius, increased with decreasing temperature in the disordered fluid state. The primary peak intensity and width show a maximum and minimum, respectively, around 80 °C. This is most likely a reflection of the glass transition of the PS cores. The sample shows an ordering transition to a bcc lattice when the volume fraction reached the value of 0.52. The core radius and volume fraction decrease upon ordering. The transformation kinetics exhibit two-stage growth, with the first stage reflecting the changes due to temperature equilibration and supercooling of the micellar fluid and the second stage corresponding to the nucleation and growth of the ordered state. The competition between the increased driving force for ordering at larger quench depths and the slowing down of the mobility, due to the formation of glassy PS cores, with decreasing temperature is reflected in the minimum in the temperature dependence of the induction time.

Acknowledgment. R.B. acknowledges the support of NSF-Div. of Materials Research (NSF-DMR Nos. 9618467 and 0217042). This work was also supported by the NSF U.S.−Czech Collaborative Research Grants (NSF INT-9600679 and ME CR ES 044). C.K. acknowledges the financial support of the Grant Agency of the Academy of Sciences of the Czech Republic (No. A4050604, A1050201, A4050305) and the Grant Agency of the Czech Republic (No. 203/03/0600). We thank Bill Klein and Tim Lodge for helpful discussions and Jun Hu for help with the SAXS measurements. We are grateful to Ben Chu, Ben Hsiao, and Fengji Yeh for support at the X27C beamline. This research was carried out at the National Synchrotron Light Source, Brookhaven National Laboratory, which is supported by the U.S. Department of Energy, Division of Materials Sciences and Division of Chemical Sciences, under Contract DE-AC02-98CH10886.

References and Notes

(1) Lai, C.; Russel, W. B.; Register, R. A. *Macromolecules* **2002**, *35*, 841−849.
(2) Hanley, K. J.; Lodge, T. P.; Huang, C.-I. *Macromolecules* **2000**, *33*, 5918−5931.
(3) Lodge, T. P.; Pudil, B.; Hanley, K. J. *Macromolecules* **2002**, *35*, 4707−4717.
(4) Hamley, I. W. *The Physics of Block Copolymers*; Oxford University Press: New York, 1998.
(5) Bates, F. S.; Fredrickson, G. H. *Phys. Today* **1999**, *52*, 32−38.
(6) Kleppinger, R.; van Es, M.; Mischenko, N.; Koch, M. H. J.; Reynaers, H. *Macromolecules* **1998**, *31*, 5805−5809.
(7) Lodge, T. P.; Xu, X.; Ryu, C. Y.; Hamley, I. W.; Fariclough, J. P. A.; Ryan, A. J.; Pedersen, J. S. *Macromolecules* **1996**, *29*, 5955−5964.
(8) Kleppinger, R.; Mischenko, N.; Reynaers, H. L.; Koch, M. H. J. *J. Polym. Sci., Part B: Polym. Phys.* **1999**, *37*, 1833−1840.
(9) Reynders, K.; Mischenko, N.; Kleppinger, R.; Reynaers, H.; Koch, M. H. J.; Mortensen, K. *J. Appl. Crystallogr.* **1997**, *30*, 684−689.
(10) Kleppinger, R.; Reynders, K.; Mischenko, N.; Overbergh, N.; Koch, M. H. J.; Mortensen, K.; Reynaers, H. *Macromolecules* **1997**, *30*, 7008−7011.
(11) Gunton, J. D.; San Miguel, M.; Sahni, P. S. In *Phase Transitions and Critical Phenomena*; Domb, C., Lebowitz, J. L., Eds.; Academic Press: London, 1983; Vol. 8.
(12) Binder, K. *Physica A* **1995**, *213*, 118−129.
(13) Fredrickson, G. H.; Binder, K. *J. Chem. Phys.* **1989**, *91*, 7265−7275.
(14) Christian, J. W. *The Theory pf Transformation in Metals and Alloys, Part I: Equilibrium and General Kinetic Theory*; Pergamon: New York, 1981.
(15) Avrami, M. *J. Chem. Phys.* **1939**, *7*, 1103.
(16) Avrami, M. *J. Chem. Phys.* **1940**, *8*, 212.
(17) Avrami, M. *J. Chem. Phys.* **1941**, *9*, 177.
(18) Adams, J. L.; Quiram, D. J.; Graessley, W. W.; Register, R. A.; Marchand, G. R. *Macromolecules* **1996**, *29*, 2929−2938.

(19) Hashimoto, T.; Sakamoto, N. *Macromolecules* **1995**, *28*, 4779−4781.
(20) Sakurai, S.; Kawada, H.; Hashimoto, T.; Fetters, L. J. *Macromolecules* **1993**, *26*, 5796−5802.
(21) Hashimoto, T.; Sakamoto, N.; Koga, T. *Phys. Rev. E* **1996**, *54*, 5832−5835.
(22) Harkless, C. R.; Singh, M. A.; Nagler, S. E.; Stephenson, G. B.; Jordan-Sweet, J. L. *Phys. Rev. Lett.* **1990**, *64*, 2285−2288.
(23) Singh, M. A.; Harkless, C. R.; Nagler, S. E.; Shannon, R. F.; Ghosh, S. S. *Phys. Rev. B* **1993**, *47*, 8425−8435.
(24) Gupta, J. A.; Singh, M. A.; Salomons, G. J.; Foran, W. A.; Capel, M. S. *Macromolecules* **1998**, *31*, 3109−3115.
(25) Sakurai, S.; Hashimoto, T.; Fetters, L. J. *Macromolecules* **1996**, *29*, 740−747.
(26) Winter, H. H.; Scott, D. B.; Gronski, W.; Okamoto, S.; Hashimoto, T. *Macromolecules* **1993**, *26*, 7236−7244.
(27) Konak, C.; Fleischer, G.; Tuzar, Z.; Bansil, R. *J. Polym. Sci., Part B*: *Polym. Phys.* **2002**, *38*, 1312−1322.
(28) Bansil, R.; Nie, H.; Li, Y.; Liao, G.; Ludwig, K.; Steinhart, M.; Konak, C.; Lal, J. *Macromol. Symp.* **2002**, *190*, 161−172.
(29) Liao, G. Kinetics of Phase Transition in Polymers, Ph.D. Thesis, Boston University, 1998.
(30) Hamley, I. W.; Fariclough, J. P. A.; Ryan, A. J.; Ryu, C. Y.; Lodge, T. P.; Gleeson, A. J.; Pedersen, J. S. *Macromolecules* **1998**, *31*, 1188−1196.
(31) Chen, W.-R.; Chen, S.-H.; Mallamace, F. *Phys. Rev. E* **2002**, *66*, 021403.
(32) Pedersen, J. S. *Adv. Colloid Interface Sci.* **1997**, *70*, 171−210.
(33) Percus, J. K.; Yevick, G. J. *Phys. Rev.* **1958**, *110*, 1−13.
(34) Mortensen, K.; Pedersen, J. S. *Macromolecules* **1993**, *26*, 805−812.
(35) Kinning, D. J.; Thomas, E. L. *Macromolecules* **1984**, *17*, 1712−1718.
(36) Schwab, M.; Stuhn, B. *Phys. Rev. Lett.* **1996**, *76*, 924−927.
(37) Wang, X.; Dormidontova, E. E.; Lodge, T. P. *Macromolecules* **2002**, *35*, 9687−9697.
(38) Yurekli, K.; Krishnamoorti, R. *Maromolecules* **2003**, *35*, 4075−4083.
(39) Steinhart, M.; Kriechbaum, M.; Horky, M.; Baldrian, J.; Amenitsch, H.; Laggner, P.; Bernstorff, S. *Adv. Struct. Anal.* **1998**, 463−472.
(40) Press, W. H.; Flannery, B. P.; Teukolsky, S. A.; Vetterling, W. T. *Numerical Recipes;* Cambridge University Press: Cambridge, 1990.
(41) Laurer, J. H.; Mulling, J. F.; Khan, S. A.; Spontak, R. J.; Lin, J. S.; Bukovnic, R. *J. Polym. Sci., Part B*: *Polym. Phys.* **1998**, *36*, 2513−2523.
(42) McConnell, G. A.; Gast, A. P.; Huang, J. S.; Smith, S. D. *Phys. Rev. Lett.* **1993**, *71*, 2102−2105.
(43) Soenen, H.; Liskova, A.; Reynders, K.; Berghmans, H.; Winter, H. H.; Overbergh, N. *Polymer* **1997**, *38*, 5661−5665.
(44) Mortensen, K.; Brown, W.; Norden, B. *Phys. Rev. Lett.* **1992**, *68*, 2340−2343.
(45) Mortensen, K. *Europhys. Lett.* **1993**, *19*, 599−604.
(46) Pusey, P. N.; van Megan, W. *Nature (London)* **1986**, *320*, 340−342.
(47) Sato, T.; Han, C. C. *J. Chem. Phys.* **1988**, *88*, 2057−2066.
(48) Ludwig, K.; Stephenson, G. B.; Jordan-Sweet, J. L.; Mainville, J.; Yang, Y. S.; Sutton, M. *Phys. Rev. Lett.* **1988**, *61*, 1859−1862.

MA034357+